Stony Brook University

Silicate-Based Thermal Spray Coatings for Environmental Protection of Silicon Carbide

A Thesis Presented

by

Ari Isaac Sagiv

to

The Graduate School

in Partial Fulfillment of the

Requirements

for the degree of

Master of Science

in

Materials Science and Engineering

(Thermal Spray Technology)

Stony Brook University

August 2011

Stony Brook University

The Graduate School

Ari Isaac Sagiv

We, the thesis committee for the above candidate for the Master of Science degree, hereby recommend acceptance of this thesis.

Dr. Christopher M. Weyant – Thesis Advisor

Assistant Professor for Materials Science and Engineering department

Dr. Dilip Gersappe

Professor for Materials Science and Engineering department

Dr. Sanjay Sampath

Professor for Materials Science and Engineering department

This thesis is accepted by the Graduate School.

Lawrence Martin

Dean of the Graduate School

Abstract of the Thesis

Silicate-Based Thermal Spray Coatings for Environmental Protection of Silicon Carbide

by

Ari Isaac Sagiv

Master of Science

In

Materials Science and Engineering

(Thermal Spray Technology)

Stony Brook University

2011

Environmental barrier coatings are a key technology for implementing ceramics in high-temperature, high-moisture environments. One such ceramic, silicon carbide, is a material that can be used in gas turbines. However, silicon carbide oxidizes into silicon dioxide with exposure to oxygen, carbon dioxide, and water vapor and would normally provide protection for the silicon carbide. However, silicon dioxide volatilizes in a gas turbine environment, which leads to the degradation of its mechanical properties, making it unfit for use in a gas turbine.

Materials like yttria-monosilicate and barium-strontium doped aluminosilicate (BSAS) both have good environmental coating properties. However, sintered yttria-monosilicate does not bond well to silicon carbide, and thermally sprayed BSAS transforms very slowly from a metastable hexacelsian phase to the desired celsian phase that is necessary for it to bond well to silicon carbide. Coatings of these materials have been produced by plasma spray with some

additional work using HVOF. Phase identification has been done by x-ray diffraction, and microstructural analysis has been done using scanning electron microscopy.

Dedication

This thesis is dedicated to the memory of

Adele Markowitz

Thank you for the gift of the power of speech.

This thesis is written in honor of

Fred and Donna Nives

Your benevolence will never go unheard.

Table of Contents

List of Figures

List of Tables

Acknowledgements

Dr. Christopher Weyant

Your guidance and mentorship has been invaluable and will always be remembered.

Dr. Sanjay Sampath

Thank you for showing confidence in me, and for showing me the roadmap to succeed.

Abraham and Susan Sagiv

Thanks to my parents, for always being by my side and supporting me.

Sharon, Abraham, Nadav and Noa Boskovitz

Michelle, Jon, Allison, and Emma Smith

Thanks to my wonderful sisters and their families, for setting a shining example.

1 Background

1.1 Introduction to Environmental Barrier Coatings

Low-density ceramics with sufficient refractory are desired for use in gas turbine engines [1]. However, maintaining a sufficient refractory is difficult because there are only a few materials that can meet the requirements. Rolls-Royce has compiled that materials with high refractory in harsh turbine conditions have high strength, good creep and oxidation resistance, and retention of strength against time and temperature [1].

Silicon carbide (SiC) is known for its low density and high refractory [2]. The substrate that is used in a combustion chamber of a gas turbine is a SiC-SiC composite. One form of SiC-SiC composites is SiC-weaved fibers melt-infiltrated with molten SiC to fill out the bulk of the material. This increases the structural integrity of the bulk material.

However, SiC oxidizes when exposed to oxygen, carbon dioxide, and water vapor, according to the chemical reactions shown in Equation 1 [3]. In many environments, the silicon dioxide provides protection to the SiC to prevent further oxidation.

Oxidation of Silicon Carbide (Equation 1)

a) $SiC\ (s) + 3CO_2\ (g) \rightarrow SiO_2\ (s) + 4CO\ (g)$

b) $SiC\ (s) + 4H_2O\ (g) \rightarrow SiO_2 + 4H_2\ (g) + CO\ (g)$

However, when SiC is exposed to an environment with high-temperature moisture moving at a high velocity, similar the conditions of a gas turbine, silicon dioxide volatilizes into silicon hydroxide ($Si_xO_x(OH)_x$), which is a gas [2]. The chemical reactions are shown in Equation 2 [3].

As the SiO_2 volatilizes, more of the SiC surface is exposed to the high-temperature, high-velocity moisture, and it continues to degrade. This causes the lifetime of the bulk material to decrease, making it inadequate for long-term applications [3].

Volatilization of Silicon Dioxide (Equation 2)

a) $SiO_2\ (s) + H_2O\ (g) \rightarrow SiO(OH)_2\ (g)$

b) $SiO_2\ (s) + 2H_2O\ (g) \rightarrow Si(OH)_4\ (g)$

c) $SiO_2\ (s) + 3H_2O\ (g) \rightarrow Si_2O(OH)_6\ (g)$

An environmental barrier coating (EBC) is designed to prevent a ceramic material from degradation by volatilization. In this case, the EBC prevents SiC from reacting with water vapor in the conditions that exist in a gas turbine combustion chamber [4]. The coating consists of one or multiple protective layers of materials that have limited or no reaction in these conditions. A successful EBC must be resistant to any form of degradation resulting from the conditions of an active gas turbine. It must also have a good refractory and chemical compatibility so that it will not react with the substrate. The coefficient of thermal expansion (CTE) of the EBC must also be compatible with the substrate in order to prevent residual stresses, which causes crack propagation [5]. Porosity and cracking must be minimized in order to prevent any degradation agents from penetrating the coating [6].

1.2 Materials used in Environmental Barrier Coatings

Two silicate materials systems were evaluated for thermally sprayed EBC's: yttria-silicate (yttria-monosilicate (Y_2SiO_5) and yttria-disilicate ($Y_2Si_2O_7$.)) and barium-strontium doped aluminosilicate (BSAS).

1.2.1 Yttria-Silicate Mixtures

Yttria-monosilicate has a low oxygen permeability over a wide temperature range and has a theoretical CTE that is close to SiC [7]. It has a low young's modulus but a very high damage tolerance. It has a very low thermal conductivity (1.34 W/(m K)) at 873 K to 1173 K, which is lower than most thermal barrier coatings [7]. However, it is very difficult to obtain pure yttria-monosilicate, and heterogeneous monosilicate can delaminate due to the differences in the CTE of its substances [7].

However, yttria-disilicate was found to have a thermal expansion coefficient that more closely matches SiC, increasing its coating stability. It can be used as a bond-coat between the substrate and yttria-monosilicate. Yttria-disilicate coating layers can support very low compressive stresses, and can preserve the integrity of the coating. [8]. A phase diagram of yttria-silicate is shown in Figure 1.

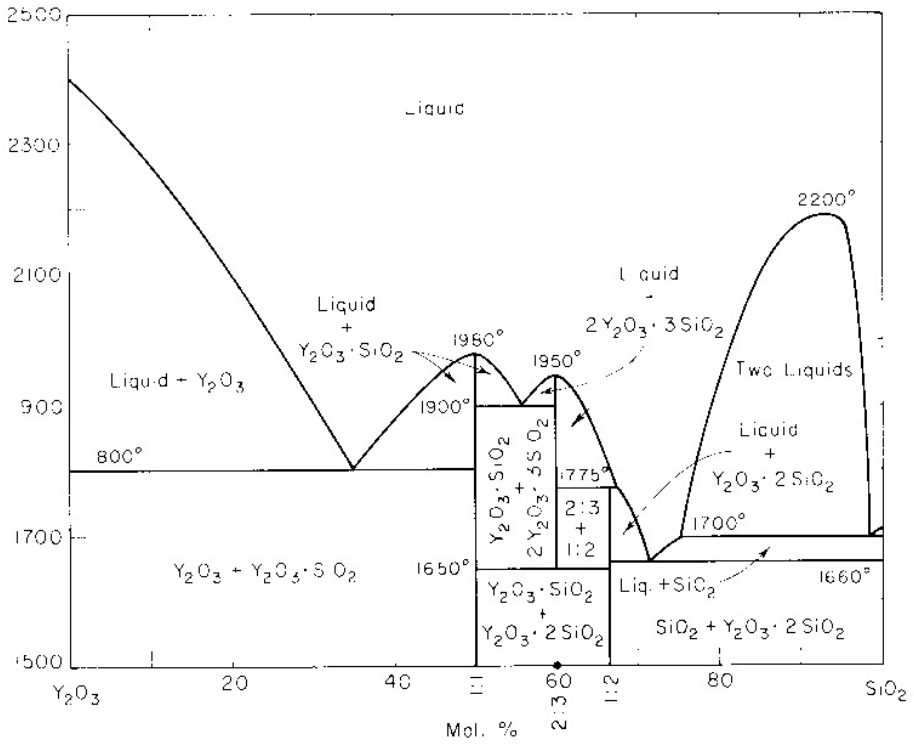

Figure 1. Yttria-silicate phase diagram. Image by Levin, *et al* [9].

1.2.2 Barium-strontium Doped Aluminosilicate (BSAS)

BSAS is known for its low volatility when exposed to water vapor [4]. The two known crystalline phases of BSAS are celsian and hexacelsian [10]. BSAS is known for its high thermochemical stability and its low silica activity, making it an ideal candidate for an EBC [10]. However, hexacelsian BSAS, which is obtained after cooling from plasma spraying, has a CTE mismatch with SiC [10]. It is necessary to obtain the celsian phase before the coating delaminates.

When BSAS is used as single-layer coating for SiC, it reacts with the thermally grown SiO_2 on the SiC. The SiO_2 diffuses into the coating, and volatilizes at high-temperature and high-moisture environments [11]. This lead to BSAS being researched as a topcoat, with mullite as a bondcoat to the SiC substrate [12]. However, when testing in high-temperature and high-

moisture conditions, a thick oxide layer formed in the substrate. When silicon was used as a bondcoat between the mullite and the SiC, the substrate did not oxidize as quickly [12].

1.3 Introduction to Thermal Spray Technology

EBCs can be applied to a substrate by thermal spray processing, which is suite of coating techniques in which melted or heated particles are sprayed onto a substrate. The impact energy of the molten or heated material causes it to impact and flatten, or "splat," onto the substrate, solidifying as it cools. These "splats" are the building blocks of the microstructure of the coating. The two types of thermal spraying in focus are atmospheric plasma spraying (APS) and high-velocity oxy-fuel (HVOF).

1.3.1 Atmospheric Plasma Spray (APS)

A plasma is induced by transferring electrical energy to an ionizing gas, usually argon or helium mixed with hydrogen [13], until the energy of the electron in the ionizing gas is high enough to have a system of positively-charged ions and free electrons [14]. The large attractive forces between the ions and the electrons cause them to re-combine, releasing enthalpy and kinetic energy to the carrier jet, forming a plasma jet [13]. The feedstock powder is fed to the plasma jet, causing the particles to melt and move at a high velocity towards the substrate. A diagram of a plasma sprayer is shown in Figure 2. A plasma jet can reach a temperature of around 15,000 K if the DC power input is 40 kW [13].

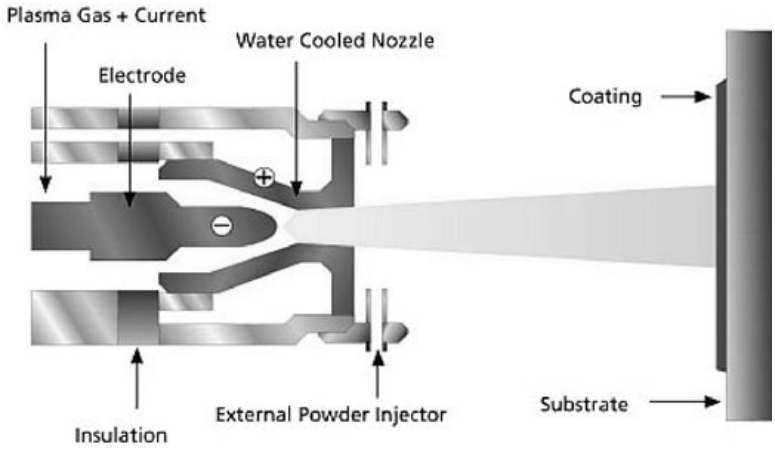

Figure 2. Plasma-spray schematic. Image by Flame Spray Technologies[15].

1.3.2 High-Velocity Oxy-Fuel (HVOF)

HVOF is derived from the D-Gun coating technique, which involves fuel combustion in a confined chamber. Instead of individual bursts of combustion, HVOF operates on a steady-state basis [14]. High-volume combustible gases are fed into a combustion chamber. The gas is ignited continuously, resulting in a jet velocity of 700-1200 mph (313-536 m/s) [16]. The supersonic nature of the jet causes shock diamonds within the jet [14]. The combusting gases for HVOF are hydrogen, alcohol, propane, kerosene, or any combination of them [16]. A diagram of HVOF is shown in Figure 3.

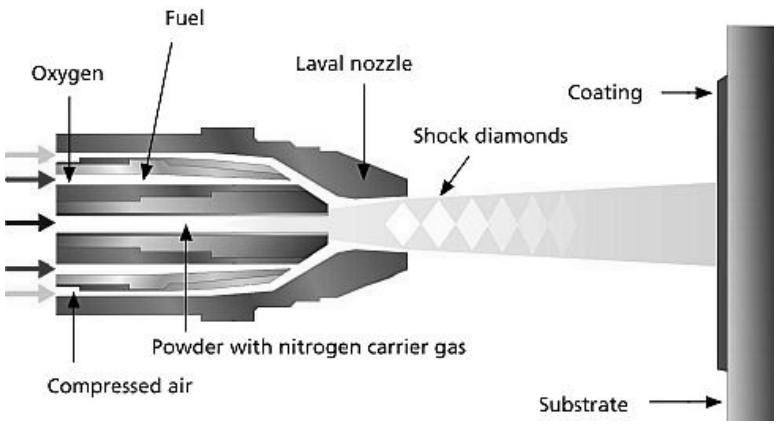

Figure 3. Schematic of HVOF Spraying. Image by Flame Spray Technologies[17].

Compared to APS, HVOF sprays at a lower temperature, which can result in more unmelted particles. The increased kinetic energy of the particle causes an increase in its impact energy, yielding a denser coating. Image analysis by Deshpande, *et al*. [18] has shown that APS sprayed coatings for yttria-stabilized zirconia yield larger globular pores, interlamellar pores, and cracks and that HVOF has well-adhered splats with finer porosity.

2 Experimental Procedure

2.1 Grit Blasting

The surface of a SiC-SiC composite is rough, which causes the coating to bond well to the substrate. However, since the composite is expensive, bulk SiC was used for coating development. It is necessary to grit-blast bulk SiC, which has a smooth surface, to emulate the surface of the composite. In order to determine the proper grit blast procedure, a design of experiments was developed (Table 1), which investigates grit type, size, blast time, and pressure.

Table 1. Grit blasting design of experiments.

Material	Grit Size (mesh)	Blast Time (mm:ss)	Blast Pressure (PSI)
Alumina	24	0:30	80
Alumina	24	1:00	80
Alumina	24	1:30	80
Alumina	24	2:00	80
Alumina	24	2:30	80
Alumina	24	5:00	80
Alumina	24	10:00	80
SiC	60	2:00	80
SiC	60	0:10	80
SiC	60	0:20	80
SiC	60	0:10	40
SiC	60	0:30	40
SiC	24	0:10	80

2.2 Pure Powder Calcination of Yttria-Silicate Mixtures

Three different mixture ratios of yttria and silica were prepared for APS and HVOF. The pseudo-binary phase diagram for yttria (Y_2O_3) and silica (SiO_2) is shown in Figure 1. The three phases synthesized by calcination are 3:1, 1:1, and 1:2 of yttria-silica. Both 1:1 and 1:2 are line compound phases of yttria-silica, which are yttria-monosilicate (Y_2SiO_5) and yttria-disilicate ($Y_2Si_2O_7$), respectively. The 3:1 mixture is a heterogeneous mixture of yttria-monosilicate and pure yttria.

The component oxides, yttria (MW = 225.8 g/mol) and silica (MW = 60.08 g/mol), were blended and calcinated at 1600 °C for 60 hours. The mole and mass ratio of each sample are shown in Table 2. After calcination, the powders were ground by mortar and pestle, and then sieved.

Table 2. Molar and mass ratios of yttria and silica.

Molar Ratio (Y_2O_3:SiO_2)	Grams Y_2O_3 per gram SiO_2
3:1	11.27
1:1	3.75
1:2	1.87

2.3 Sol-Gel Synthesis of Yttria-Silicate Mixtures

Sol-gel synthesis offers a promising method of silicate powder production. When tetraethylorthosilicate (TEOS) is exposed to water, it forms silica by hydrolysis [19]. The sol-gel reaction is shown in Figure 4. The addition of yttrium nitrate ($Y(NO_3)_3$) to this reaction results in a yttria-silicate mixture [20, 21]. The advantages of sol-gel over pure calcination are:

- Better homogeneity is ensured due to nucleation of powders instead of diffusion and sintering [19].
- Lower calcination temperature at 1100 °C (vs. 1600 °C for pure powder) [20, 21].

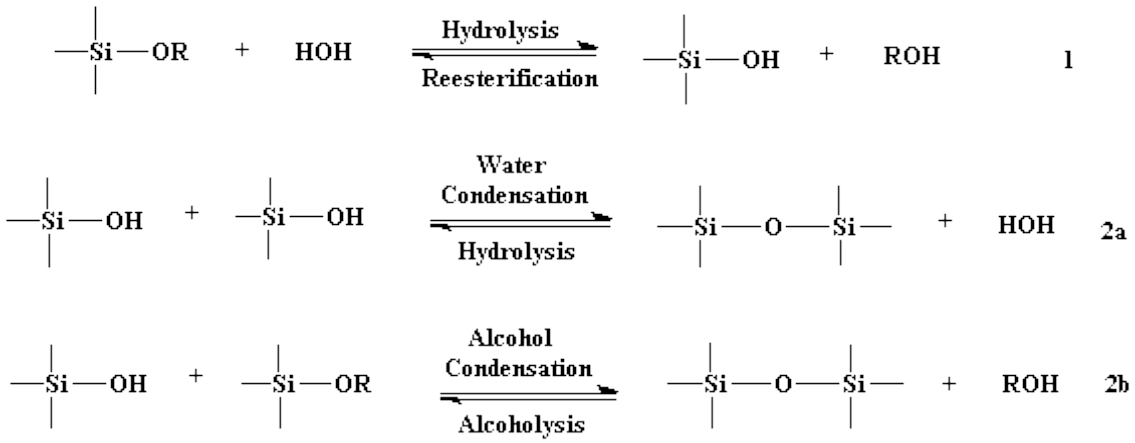

Figure 4. Sol-gel synthesis reaction. Image by The University of Southern Mississippi[22].

The synthesis of yttria-disilicate was done by sol-gel method as outlined by Moya, *et al*. [21] and Diaz, *et al.* [20]. This method involves dissolving yttrium nitrate $Y(NO_3)_3$ in a hydrochloric acid (HCl) solution, and mixing it with TEOS diluted in ethanol. The solvent was then evaporated, leaving a sol-gel precursor. The precursor was then dried in an oven at 100 °C for 24 hours, and calcinated at 1100 °C, with a ramp rate of 4 °C per minute and a dwell time of 2 hours.

A 3-level full factorial design of experiments was formulated based on variables that may affect the composition of the final powder based on preliminary experiments and possible factors outlined by Moya, *et al*. [21] and Diaz, *et al.* [20]. The factors and their levels are shown in Table 3. The pH of the solvent plays an important role, because HCl is the catalyst of the sol-gel

reaction. It is also possible that a different volume of the same proportions of the reactants may yield different product ratios. Preliminary experiments have also shown that the solvent evaporates when left open, so covering it may be necessary to ensure all reactants are present during the sol-gel reaction.

Table 3. Design of experiments for sol-gel synthesis of yttria-silicate.

Factor	Level 1	Level 2
Solvent pH	0.0	1.2
Initial Volume of Solvent	20 mL	40 mL
Covered Beaker	Yes	No

The measurement of the responses of the design of experiments were made using Equations 3 and 4:

- Total weight loss during processing (Equation 3).

$$\%\text{Wt. Loss} = \frac{\text{Wt. of precursor after synthesis}}{\text{Initial weight of reactant}} \times \frac{\text{Final weight of powder}}{\text{Wt. of precursor before calcination}}$$

- Yttria-monosilicate to yttria-disilicate ratio (Equation 4).

$$\text{Ratio of Monosilicate to Dislilcate} = \frac{\text{Height of monosilicate peak}}{\text{Height of disilicate peak}}$$

2.4 Thermal Spraying of Yttria-Silicate powders

The conditions used for the plasma spraying of yttria-silicate are shown in Table 4. The plasma torch used was a Sulzer 3MB. Each of the three mixture ratios mentioned in section 2.2 were sprayed onto a grit-blasted SiC substrate. The substrates were preheated to 750 °C before spraying. Sometimes after spraying, the substrate would be heat-treated with the plasma torch to crystallize any amorphous particles.

Aside from using the Sulzer 3MB plasma torch, an alternative torch provided by MesoScribe™, called Mesoplasma™, was used to plasma spray yttria-silicate onto SiC. Mesoplasma™ has a smaller nozzle than the Sulzer 3MB, and therefore has a higher particle velocity, allowing for a denser coating while maintaining the high temperatures achieved in plasma spraying.

Table 4. Plasma spray processing parameters for yttria-silicate.

Parameter	Setting
Torch Current	600 A
Torch Voltage	65 V
Primary Argon Flow	37.76 SLM (80 scfh)
Secondary Hydrogen Flow	7.08 SLM (15 scfh)
Spray Distance	3 inches
Argon Carrier Flow	~3.77 SLM (~8 scfh)
Powder Feed Rate	~10 g/min

Bi-layer yttria-silicate coatings were used because of the distinct properties of yttria-monosilicate and yttria-disilicate. Yttria-disilicate was found to have better adhesion properties to SiC than yttria-monosilicate, and yttria-monosilicate is not as susceptible to degradation as yttria-disilicate [8]. So the yttria-disilicate bondcoat was sprayed using Mesoplasma™, while the yttria-monosilicate topcoat was sprayed with either Mesoplasma™ or HVOF.

2.5 Post-Spray Heat Treatment of Yttria-Silicate

Plasma spraying of yttria-silicate coatings results in porosity due to unmelted particles and cracks due to residual stresses. In order to optimize the EBC, heat-treatments were performed at 1200 °C for 48 hours, with a ramp speed of 4 °C/min. The bi-layer coating was put under a thermal cycle process: 165 cycles of a 15 minute soak at 1150 °C and a 5 minute air cool. This was to test the longevity of the coating under the conditions of a gas turbine, which has continuous heating and cooling. The thermal cycle temperature versus time is shown in Figure 5.

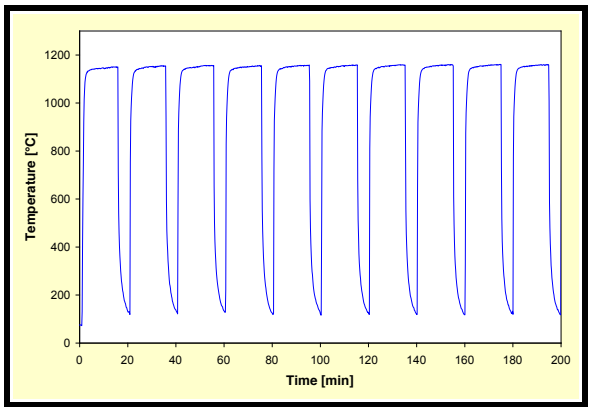

Figure 5. Thermal cycle process of the yttria-silicate bi-layer coating.

2.6 Kinetic Study and Pre-Spray Preparation of BSAS

BSAS in its stable celsian phase has a CTE of 4.0-5.15 x 10^{-6} °C^{-1}, which is compatible with SiC (CTE = 5.7 x 10^{-6} °C^{-1}) [10]. Previous experiments by Harder, *et al*. [10], shows that plasma-sprayed celsian BSAS becomes amorphous due to melting and rapid cooling. When heat-treating amorphous BSAS at 990 °C for 10h, the BSAS transforms to the metastable hexacelsian phase [10]. Hexacelsian BSAS has a CTE of 7.5-8.0 x 10^{-6} °C^{-1}, a significant difference from SiC.

A design of experiment was previously performed based on the data by Harder, *et al*., to attempt to obtain celsian BSAS from amorphous BSAS. The design of experiments is shown in Table 5. After obtaining only the hexacelsian phase of BSAS for all experiments, a second set of experiments were done to see if it was possible for a phase change to occur. These experiments are shown in Table 6.

Table 5. Initial design of experiments for heat-treatment of amorphous BSAS.

Temperature (°C)	Time (hours)
1000	2
1000	3
1000	4
1100	2
1100	3
1100	4
1200	2
1200	3
1200	4

Table 6. Secondary design of experiments for heat-treatment of amorphous BSAS. (Starred samples were heat-treated at Northwestern University).

Temperature	Time (hours)	Temperature	Time (hours)
1000	12	**1200**	24
1000	48	**1200**	48
1100	12	**1200**	72
1100	48	**1300***	2
1100	72	**1300***	4
1200	8	**1300***	8
1200	10	**1300***	24
1200	12		

A series of x-ray scans were performed on known mixed percentages of hexacelsian and celsian BSAS, so that a quantitative percentage of celsian BSAS can be determined from a single

x-ray spectrum. Table 7 shows the quantity of each phase of BSAS mixed, along with the known percentage of celsian BSAS, which is calculated with Equation 5 (m being the mass of each material).

$$Known\ \%\ Celsian\ BSAS = \frac{m_{Celsian}}{m_{Celsian} + m_{Hexacelsian}}$$

Table 7. Design of experiment for known percentages of Celsian BSAS.

Celsian BSAS (grams)	Hexacelsian BSAS (grams)	Percent Celsian BSAS
0.5	4.5	90 %
1.5	3.5	70 %
2.5	2.5	50 %
3.5	1.5	30 %
4.5	0.5	10 %

2.7 Plasma Spraying of BSAS

After an understanding of the phase transformation kinetics of BSAS has been achieved, plasma spraying was conducted to determine phase composition of a BSAS coating. The coatings are sprayed with the parameters shown in Table 8:

Table 8. Plasma spray parameters for BSAS.

Parameter	Setting
Primary Argon Flow	37.5 SLM
Secondary Hydrogen Flow	6.0 SLM
Powder Feed Rate	~20 g/min
Raster Speed	500 mm/s
Substrate Preheat Temp.	1000 °C

The variation of the spray parameters in the design of experiment for the plasma spraying of BSAS are the arc current, the distance between the torch and the substrate, number of passes the torch makes over the substrate, and the phase of the powder sprayed. Table 9 shows the design of experiments.

Table 9. Design of experiments for plasma spraying of BSAS.

Sample #	Arc Current (A)	Spray Distance (mm)	Number of Passes	Powder Phase
1	550	170	11	Amorphous
2	550	70	11	Amorphous
3	550	170	6	Amorphous
4	550	100	5	Amorphous
5	600	100	5	Amorphous
6	650	100	5	Amorphous
7	550	100	5	Celsian
8	600	100	5	Celsian
9	650	100	5	Celsian
10	550	170	5	Celsian

3 Results and Discussion

3.1 Grit Blasting

Grit blasting was done with Al_2O_3 and SiC grits in order to roughen the surface of bulk SiC substrate. Table 8 shows the results of the grit blast study. 24-grit alumina (Al_2O_3) was the initial designated grit material for roughening the bulk SiC. However, the 3:1 Y_2O_3:SiO_2 immediately delaminated from the Al_2O_3 grit-blasted surface when plasma sprayed, and yttria-monosilicate delaminated during post-spray processing. In order to obtain a rougher surface, a harder material was needed to match the hardness of SiC. The testing of 60-grit SiC yielded a slightly higher roughness than 24-grit Al_2O_3 at the same pressure. However, 24-grit SiC had a roughness that was double the amount of 24-grit Al_2O_3. The complete grit blast design of experiments and their results are shown in Table 10.

Table 10. Results of grit-blast study on SiC substrate.

Grit Material	Grit Blast Pressure (PSI)	Grit Blast Time (mm:ss)	Average Roughness (µm)	Standard Deviation (µm)
24-Grit Al_2O_3	80	0:30	1.83	0.38
24-Grit Al_2O_3	80	1:00	1.83	0.16
24-Grit Al_2O_3	80	1:30	2.04	0.16
24-Grit Al_2O_3	80	2:00	2.21	0.45
24-Grit Al_2O_3	80	2:30	2.35	0.42
24-Grit Al_2O_3	80	5:00	2.19	0.36
60-Grit SiC	80	0:10	2.64	0.31
60-Grit SiC	80	0:20	2.52	0.15
60-Grit SiC	40	0:10	1.30	0.32
60-Grit SiC	40	0:30	1.42	0.13
24-Grit SiC	80	0:10	5.01	0.09
24-Grit SiC (45° impact angle)	80	0:10	3.83	0.26

The pressure was modified in order to determine if it had an important effect on the roughness of the substrate. A high grit-blast pressure performed better, because the kinetic energy of the grit particles determines how much material is removed from the substrate. With increased impact energy transferred from the kinetic energy of the particle, more material is removed from the substrate. The impact angle was also tested. All samples were grit blasted perpendicular to the surface of the substrate, with the exception of one, which was grit-blasted from a 45-degree angle. The roughness of the 45-degree grit blasted sample was less than that of the perpendicular grit-blasted sample.

3.2 Sol-Gel Synthesis of Yttria-Silicate

The preliminary sol-gel synthesis experiments were based on Moya, *et al*. [21] and Diaz, *et al.* [20]. Yttrium-nitrate hexahydrate ($Y(NO_3)_3$-$6H_2O$) was the initial reactant, but it required too much HCl to turn into a precursor. Yttrium-nitrate tetrahydrate ($Y(NO_3)_3$-$4H_2O$) was easier to synthesize because a lower concentration of HCl (pH = 1.2) yielded a precursor. The precursor generally has lots of extra mass, due to it possibly being a hydrate. However, calcination removes all the extra mass.

After performing x-ray diffraction of the calcinated powder, it was determined that it was yttria-monosilicate (JCPDS 41-0004). The x-ray spectrum is shown in Figure 6. This is unusual, since the method outlined by Moya, *et al.* [21] and Diaz, *et al*. [20] results in yttria-disilicate. Repetition of this experiment shows the same result. The quantity of TEOS was doubled in the next preliminary experiment, but x-ray diffraction showed the final powder was a mixture of yttria-monosilicate and yttria-disilicate, as shown in Figure 7. Based on these results, it is

possible that there could be an environmental factor during mixing that is impeding on SiO_2 formation, leaving a surplus of Y_2O_3.

The raw data for the design of experiments is shown in Table 11. The experiments were randomized and analyzed with Minitab™. Though the results show that there is some difference in weight loss and monosilicate-disilicate ratio, none of the differences are significant on a 90-percent confidence interval. Having done a process optimization in Minitab™, the following conclusions were made based on the sol-gel process:

- A higher pH leads to more yttria-monosilicate.
- A higher initial solvent volume leads to less weight loss and a more yttria-monosilicate.
- Covering the solution does not affect the ratio of yttria-monosilicate to yttria-disilicate, but it does reduce the weight-loss during processing.

Due to the lack of consistent results and overall quantity, none of the sol-gel synthesized yttria-silicate powders were thermally sprayed.

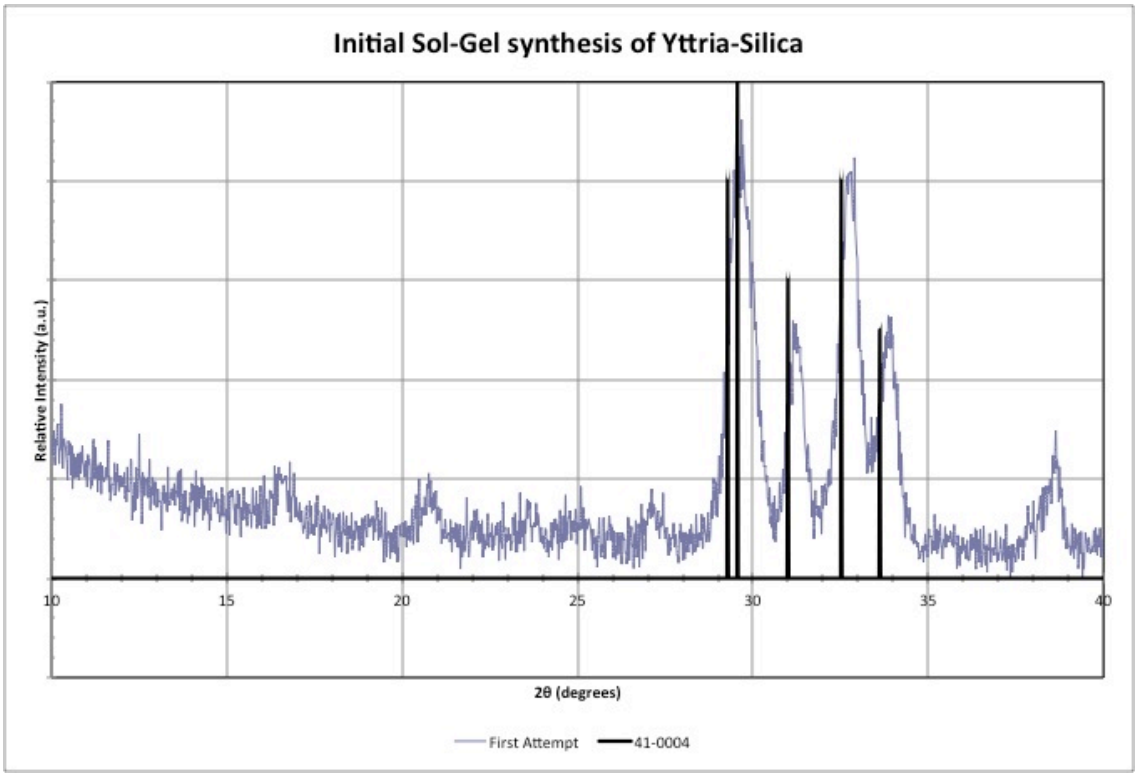

Figure 6. X-ray spectrum of initial sol-gel synthesis. "41-0004" is the JCPDS diffraction data for yttria-monosilicate[23].

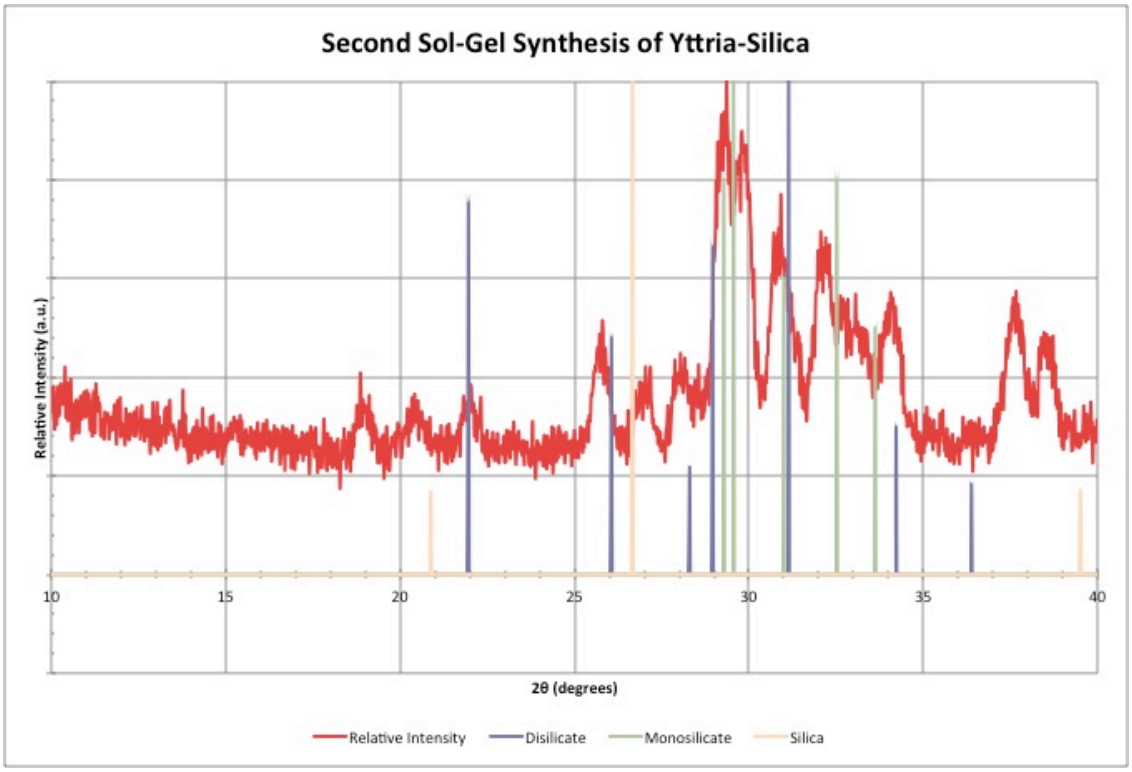

Figure 7. X-ray spectrum of second sol-gel synthesis (2X quantity TEOS).

Table 11. Design of experiments for sol-gel synthesis of yttria-silicate.

Run Order	pH	Quantity	Cover	Mono/Di	% W.L.
1	0	40	No	0.81	0.556
2	1.2	40	No	0.83	0.562
3	0	20	No	2.76	0.596
4	1.2	40	Yes	0.85	0.536
5	1.2	20	No	5.59	0.621
6	1.2	20	Yes	0.56	0.545
7	0	40	Yes	6.23	0.548
8	0	20	Yes	8.54	0.549

3.3 Thermal Spraying of Yttria-Silicate

3.3.1 APS of Yttria-Silicate powders

The preliminary APS of yttria-silicate showed that 3:1 yttria-silicate did not adhere to the substrate, delaminating almost immediately after spraying. This is because, according to the phase diagram in Figure 3 [9], 3:1 is a mixture of pure yttria and yttria-monosilicate. Pure yttria has a CTE of 8.1 x 10^{-6} K^{-1} [24] while SiC has a CTE of 5.7 x 10^{-6} K^{-1} [10]. The CTE mismatch causes residual stresses that results in the delamination of the coating.

APS of yttria-monosilicate on a 750 °C pre-heated SiC substrate with a low-roughness showed a good coating deposition, but poor adhesion after it cooled down. Using 24-grit SiC to grit blast the SiC substrate greatly increased the roughness, as well as the adhesion of yttria-monosilicate. Yttria-disilicate adhered well to both low and high roughness surfaces after pre-heating at 750 °C.

Figure 8 shows a SEM image of yttria-monosilicate sprayed onto a 24-grit SiC blasted SiC substrate. The image shows many through-thickness cracks and some separation between the

coating and the substrate. It is possible that the cracks and delamination are due to the internal stresses caused by the differences in the CTE of the heterogeneous mixture in yttria-monosilicate. Figure 9 shows a close-up of the microstructure of yttria-monosilicate. The lightest area is pure yttria, which highly contrasts in CTE from yttria-monosilicate (5-6 x 10^{-6} K^{-1} [4]) and yttria-disilicate (3.9 x 10^{-6} K^{-1} [7]). One possible reason for the low degree of homogeneity is that calcination alone does not fully diffuse silica and yttria. Sun, *et al*. mentions that single-phase yttria-monosilicate is very difficult to synthesize. Impurities have a very strong influence on the coefficient of thermal expansion. Instead of the theoretical CTE of 5-6 x 10^{-6} K^{-1}, the measured CTE of heterogeneous yttria-monosilicate is 8.36 x 10^{-6} K^{-1} [7].

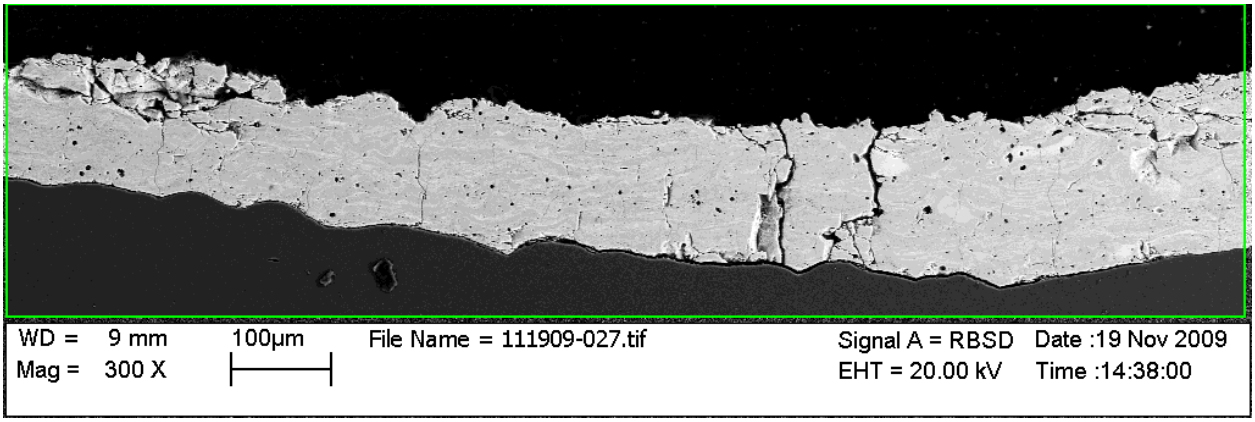

Figure 8. SEM image of yttria-monosilicate plasma sprayed onto SiC substrate.

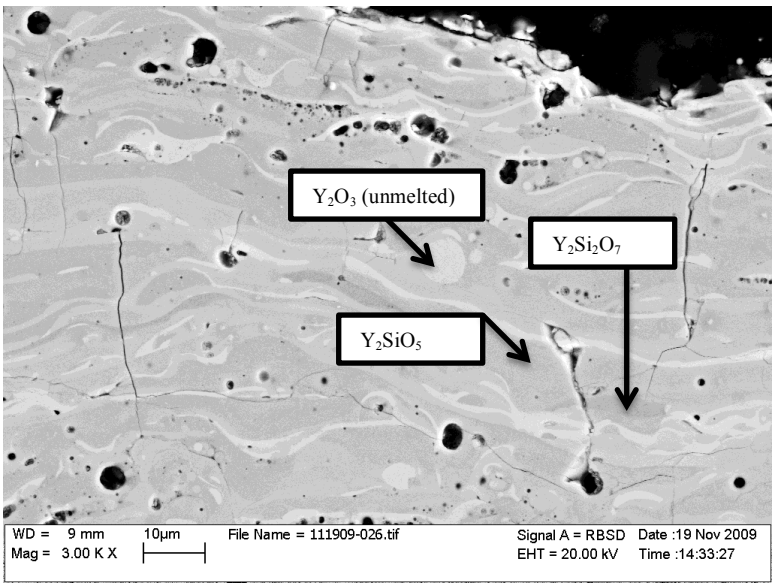

Figure 9. SEM image of microstructure of yttria-monosilicate deposit.

Yttria-disilicate was also heterogeneous, but is less likely to contain pure yttria. The yttria-disilicate heterogeneous mixture did not delaminate as easily as yttria-monosilicate, because yttria-disilicate and yttria-monosilicate do not have distinct coefficients of thermal expansions from silicon carbide.

The SEM image of the yttria-disilicate coating is shown in Figure 10. Compared to the yttria-monosilicate shown in Figure 8, yttria-disilicate has smaller through-thickness cracks and much better adhesion to the substrate. Figure 11 shows a close-up of Figure 10. There are still some traces of pure yttria, though not as much as the yttria-monosilicate in Figure 8. The pure yttria may explain why there are still some through-thickness cracks in the deposit.

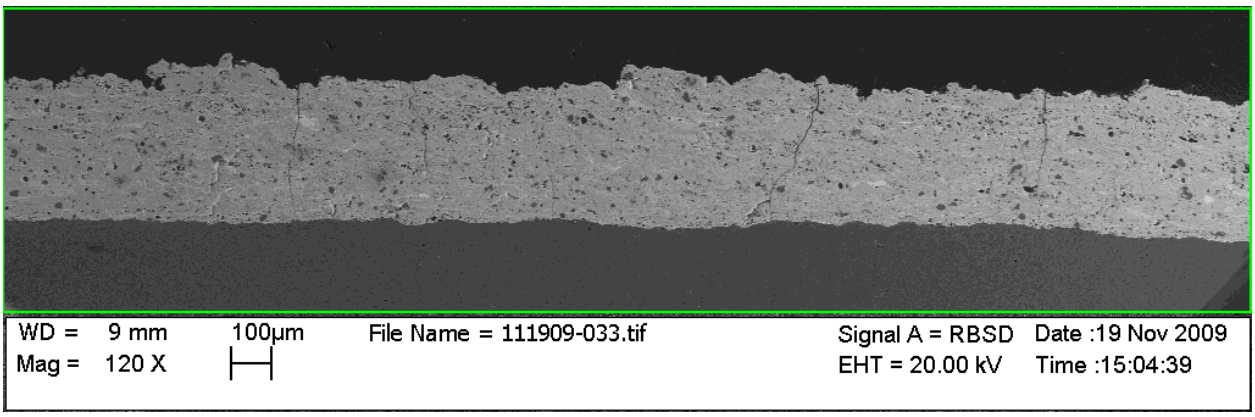

Figure 10. SEM image of yttria-disilicate plasma sprayed onto SiC substrate.

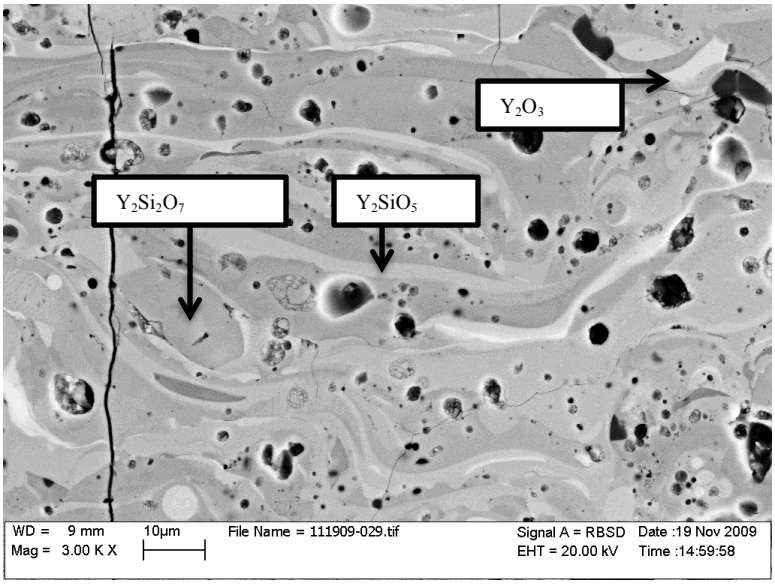

Figure 11. SEM image of yttria-disilicate deposit microstructure.

3.3.2 Heat Treatment of Thermally Sprayed Yttria-Silicate Coatings

Since through-thickness cracks are detrimental to a good environmental barrier coating, it is necessary to heat-treat the coating in order to sinter those cracks. The sample was placed in a tube furnace for 48 hours at 1200 °C. Figure 12 shows a SEM image of yttria-monosilicate

before heat-treatment. There are lots of microcracks in the structure due to the residual stress. The heat-treatment not only sinters the microcracks, but also allows for the interdiffusion of atoms within the coating, reducing the residual stress. This is evidenced by the image shown in Figure 13, which is a heat-treated version of the previous sample. There are still visible microcracks in the heat-treated microstructure, but not as large as in Figure 12.

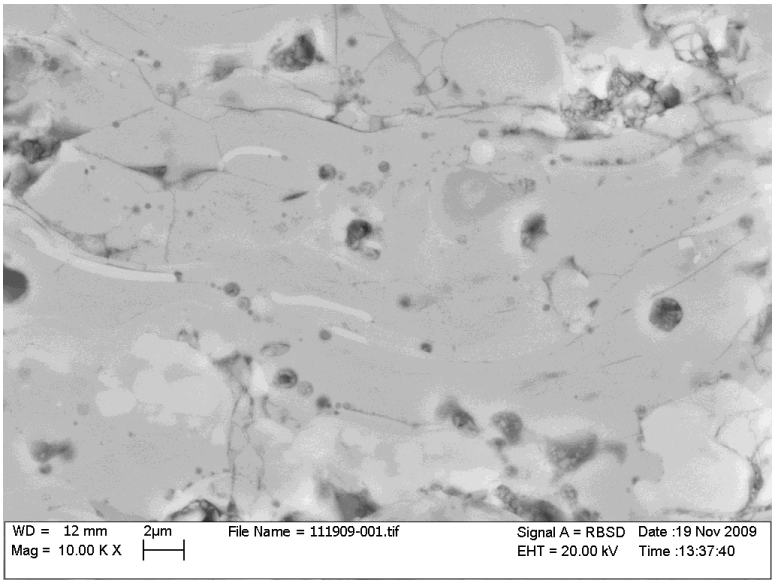

Figure 12. Yttria-monosilicate before heat-treatment.

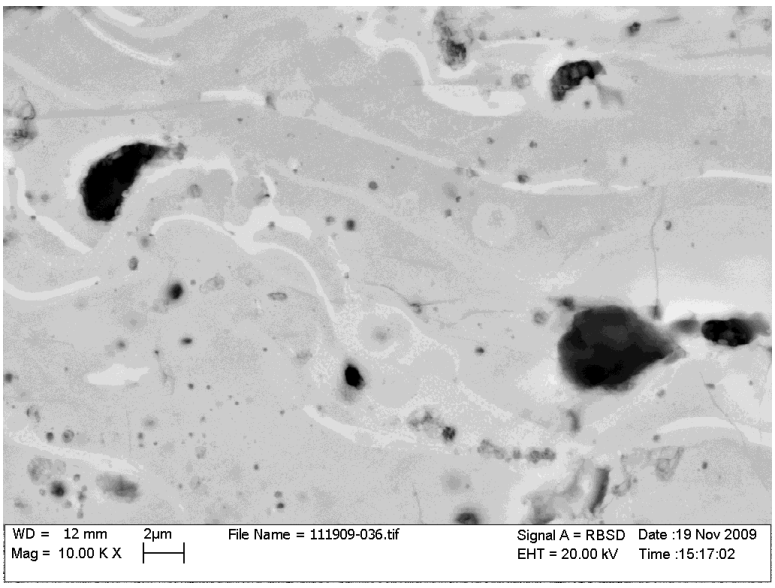

Figure 13. Yttria-monosilicate coating after heat-treatment.

3.3.3 MesoPlasma™ sprayed Yttria-Silica.

Figures 9 and 11 show that there is high porosity in both plasma sprayed yttria-monosilicate and yttria-disilicate. Pores usually result from a low impact energy, which doesn't allow the melted splats to fill any surface voids on the deposit. Mesoplasma™ is a version of APS that utilizes a smaller nozzle, and therefore results in a higher jet velocity than regular APS.

However, because of the particle is still very hot when impacting on the substrate, it quenches and remains amorphous. The top two x-ray spectra in Figure 14 shows that there are a many peaks underneath the narrow ones. However, after heat-treating for 48 hours at 1200 °C, the amorphous parts of the coating crystallized. Figure 15 shows an SEM microstructure of as-sprayed yttria-monosilicate by MesoPlasma™. The pore density is a lot less than that of as-sprayed yttria-monosilicate by APS.

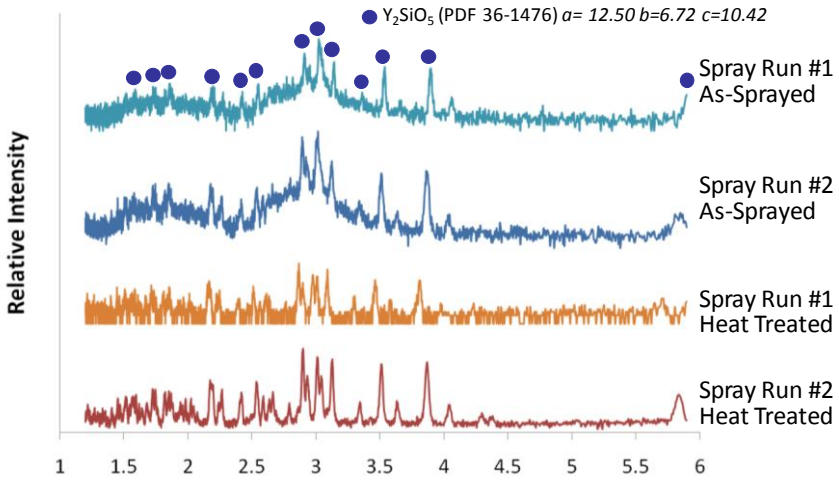

Figure 14. X-ray spectra of as-sprayed and heat-treated MesoPlasma™ sprayed yttria-monosilicate.

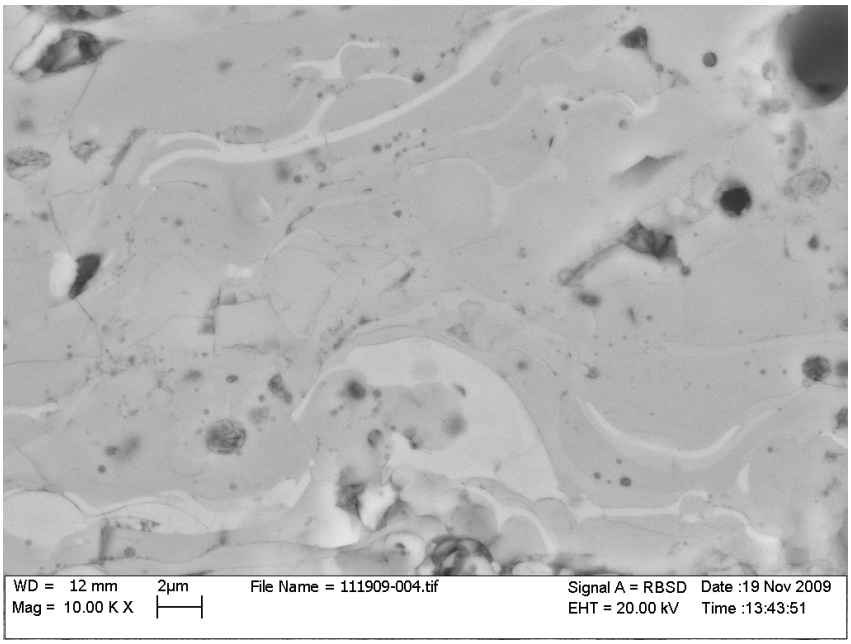

Figure 15. SEM image of MesoPlasma sprayed yttria-monosilicate.

3.3.4 Duplex Yttria-Silicate Coatings

Yttria-disilicate bonds very well to SiC. However, in the presence of high moisture, yttria-disilicate volatilizes to yttria-monosilicate and silicon hydroxide. When this happens, the coating becomes more porous, increasing the permeability of moisture and carbon dioxide. Yttria-monosilicate has the better environmental resistance of the two yttria-silicates, but it does not bond well to SiC as well as yttria-disilicate [8].

The solution to a well-formed EBC is a dual-layer coating. Yttria-disilicate acts as the bondcoat, and yttria-monosilicate is the topcoat. The MesoPlasma sprayer is used to deposit the yttria-disilicate bondcoat, and either MesoPlasma or HVOF is used to deposit the yttria-disilicate topcoat. HVOF is used to spray the topcoat, because coatings by HVOF are much more dense than APS and MesoPlasma.

Figure 16 shows the SEM image of the MesoPlasma sprayed topcoat and bondcoat. There are lots of through-thickness cracks in the topcoat, but almost no cracks in the bondcoat. The cracks in the topcoat could be the result of the CTE mismatch between the topcoat and the bondcoat. Figure 17 shows a close-up of an inter-layer crack. As mentioned in section 3.3.1, the heterogeneity of the yttria-monosilicate and the heavy presence of pure yttria affect the CTE. The through-thickness and inter-layer cracks are formed due to that difference in CTE.

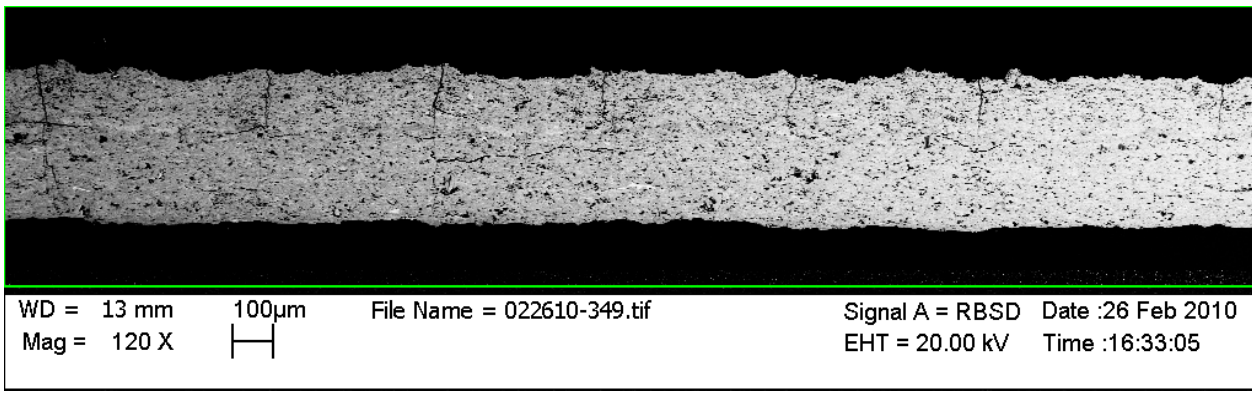

Figure 16. Duplex MesoPlasma™ topcoat and bondcoat.

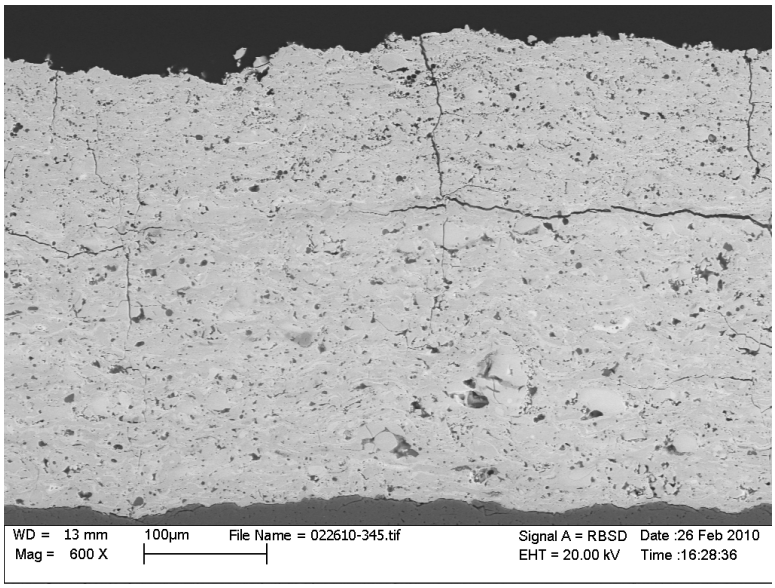

Figure 17. Close-up of dual-layer yttria-silicate coating, both sprayed by MesoPlasma™.

Figure 18 shows the cross-section of a duplex HVOF yttria-monosilicate topcoat and a MesoPlasma sprayed yttria-disilicate bondcoat. The HVOF sprayed topcoat is much more dense than the MesoPlasma sprayed topcoat. There are far fewer pores in the HVOF topcoat than the MesoPlasma topcoat. However, the number of overall cracks in the coating has not decreased. Figure 19 shows that the microcracks in the HVOF layer does not propagate into the bondcoat

layer. However, after heat-treatment at 1200 °C for 48 hours, the residual stress caused by the CTE mismatch of the material causes the crack to propagate into the bondcoat layer, as shown in Figure 20.

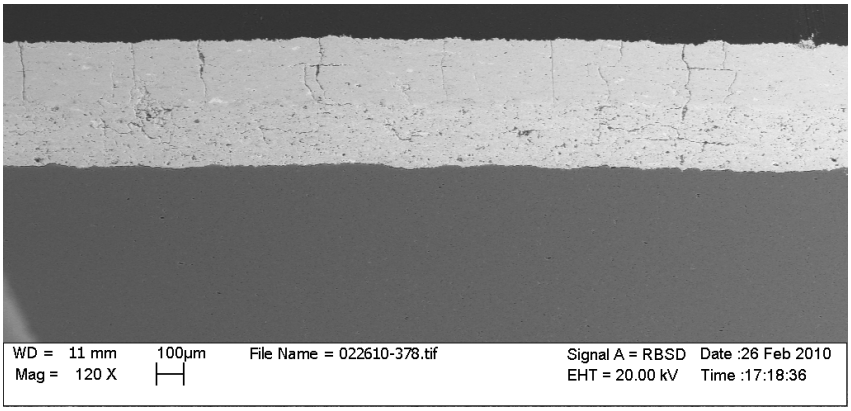

Figure 18. Duplex HVOF topcoat and MesoPlasma™ bondcoat.

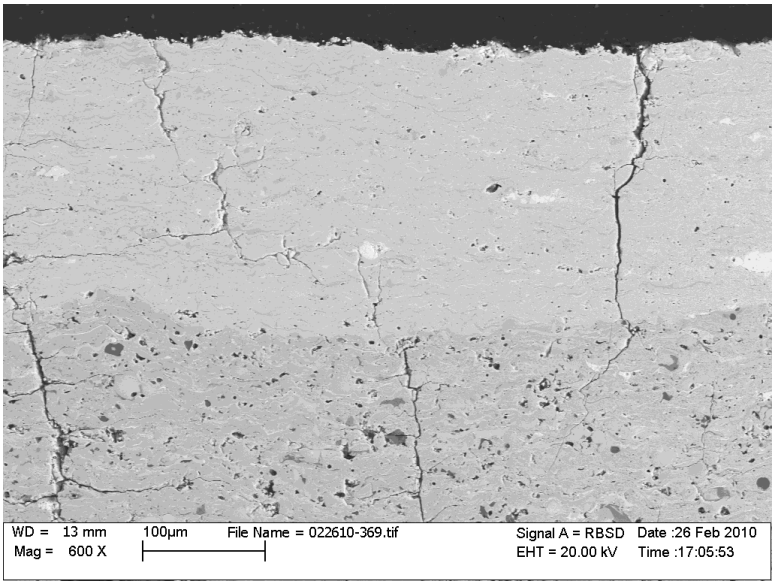

Figure 19. Close-up of duplex HVOF topcoat and MesoPlasma™ bondcoat.

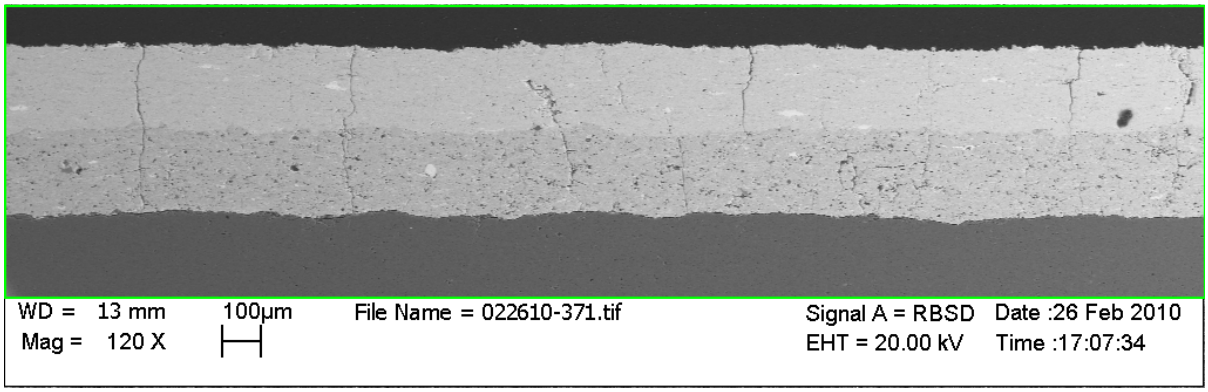

Figure 20. Heat-treated duplex coating with HVOF sprayed topcoat.

3.3.5 Thermal Cycling of Duplex Coating

Figure 5 in section 2.5 shows the thermal cycling of the bondcoat in a tube furnace. The coating did not spall after 165 cycles. However, through-thickness cracks were observed, as shown in Figure 21.

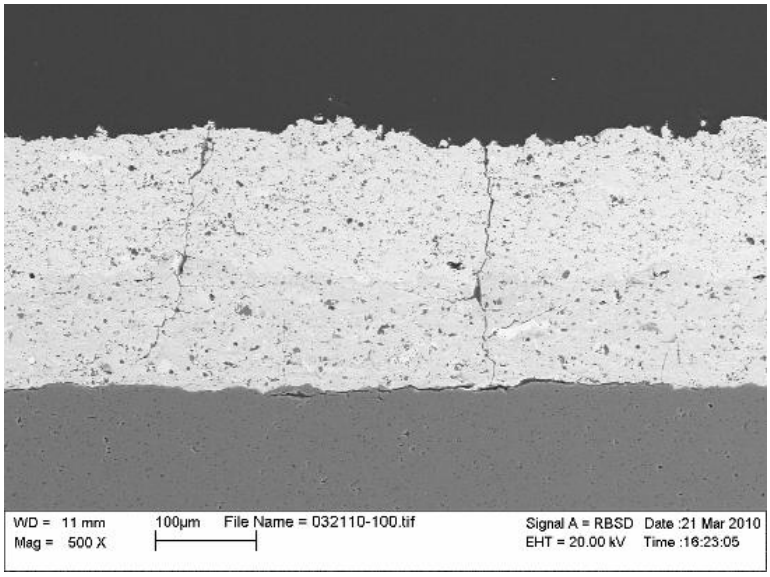

Figure 21. Thermally cycled duplex MesoPlasma sprayed coating.

3.4 Study of Kinetics of BSAS

The initial design of experiments was created to determine how quickly amorphous BSAS transformed to the hexacelsian phase at various temperatures. According to Harder, *et al*. [10], BSAS transforms from amorphous to hexacelsian phase at 990 °C. After heat-treating and performing x-ray spectra, it was determined that all experiments on Table 5 yielded hexacelsian BSAS, and in order to obtain pure hexacelsian BSAS, you would need to only heat-treat amorphous BSAS for 2 hours at 1000 °C.

The secondary design of experiments was used to determine if it was possible to obtain the celsian phase, the phase desired for the BSAS coating on SiC, from amorphous BSAS. Harder, *et al*., determined that celsian BSAS could be obtained at 1200 °C [10]. When heat-treating at 24 hours for 1200 °C, the celsian phase was dominant, but there were still traces of the hexacelsian phase. Pure celsian BSAS was attained at 1200 °C for 48 hours, and 1300 °C for 8 hours. Figures 22-25 show the results of the x-ray scans for each temperature with respect to time.

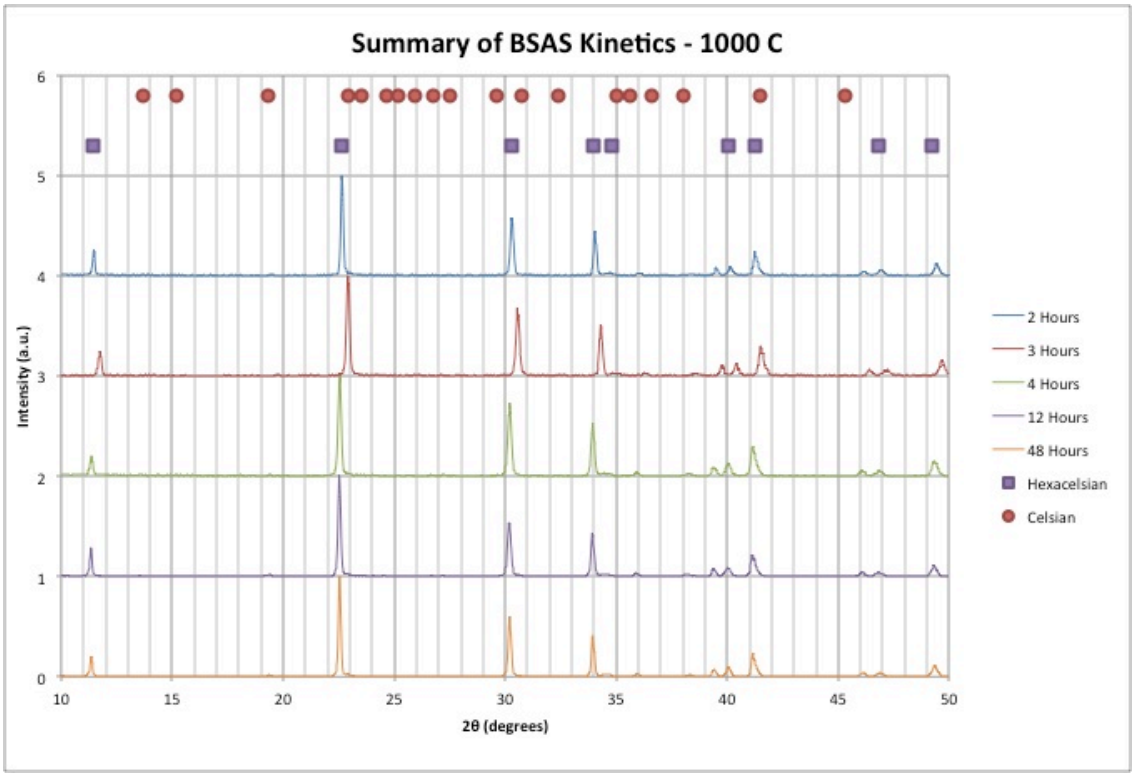

Figure 22. X-ray spectra of BSAS crystallization at 1000 C.

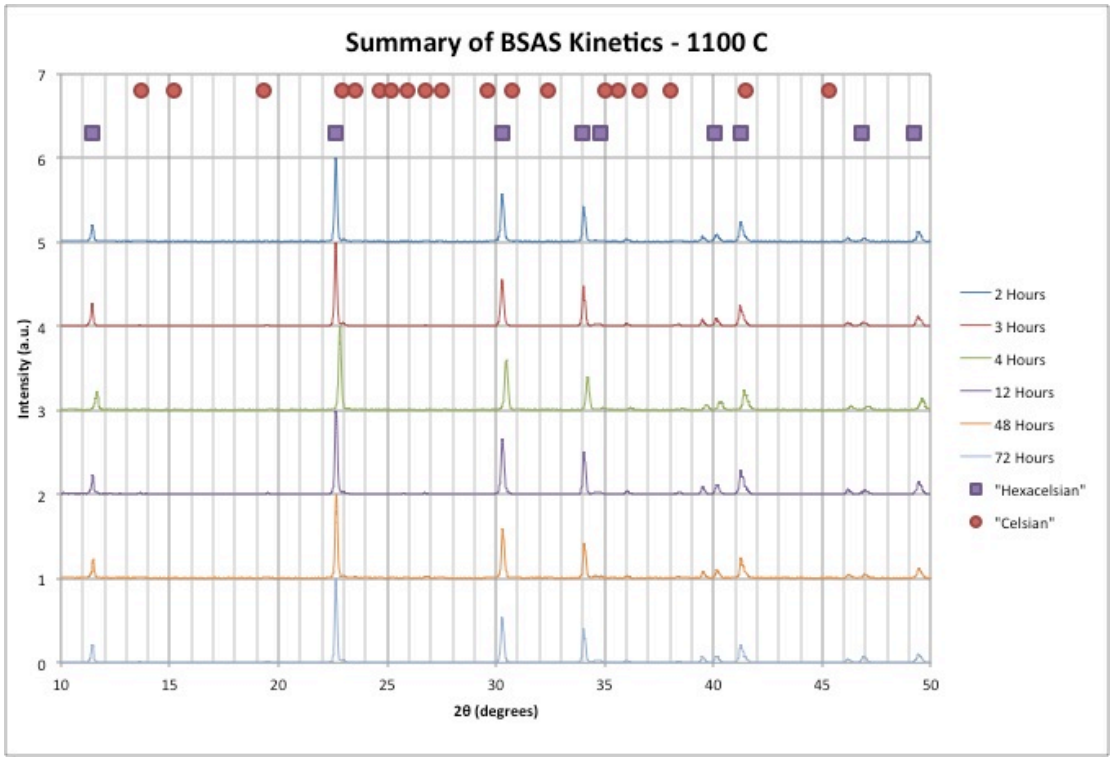

Figure 23. X-ray spectra of BSAS crystallization at 1100 C.

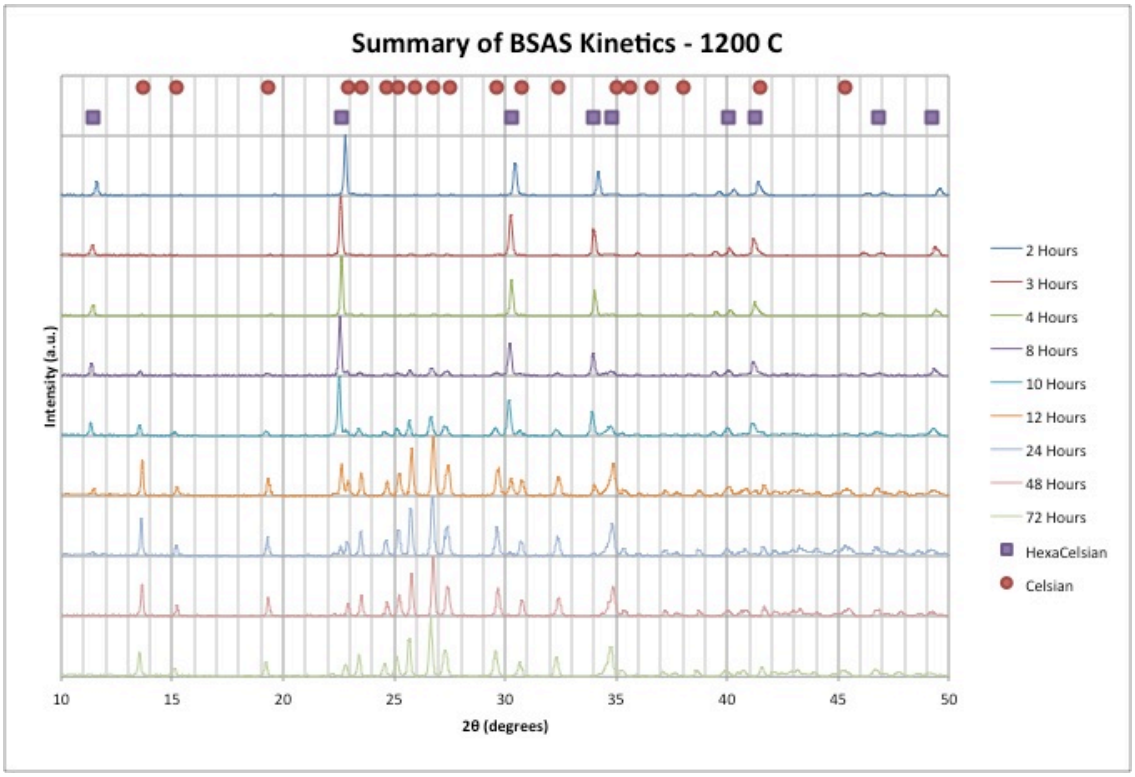

Figure 24. X-ray spectra of BSAS crystallization at 1200 C.

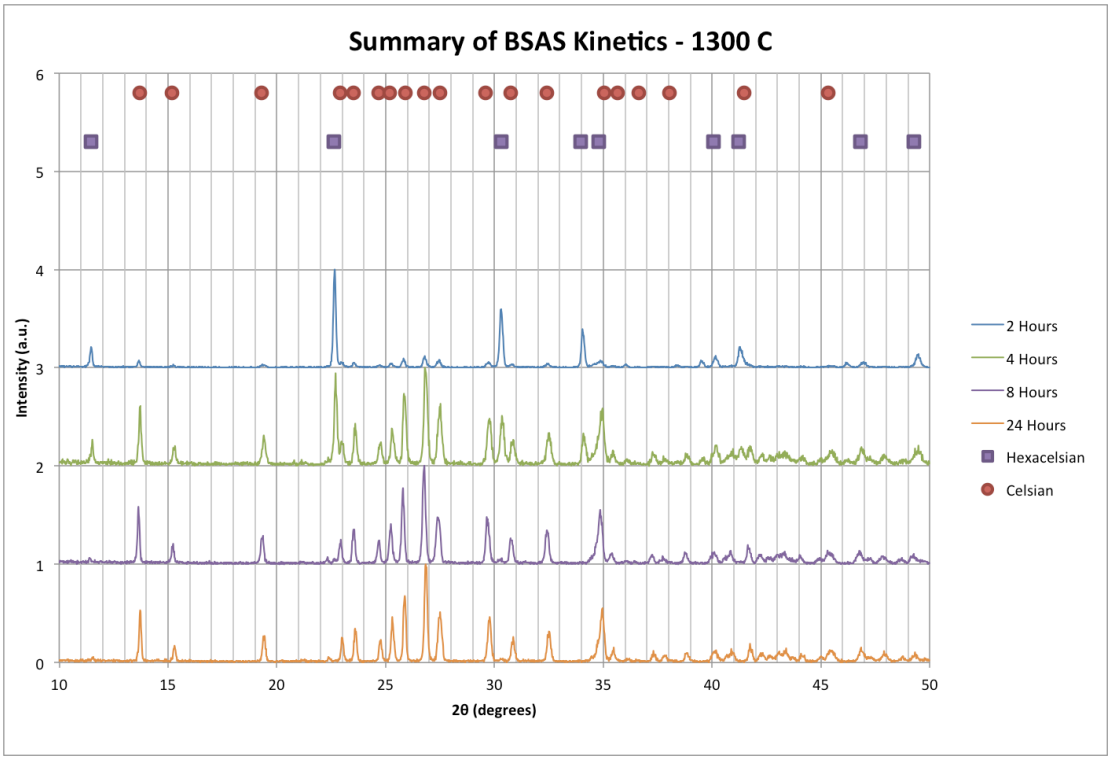

Figure 25. X-ray spectra of BSAS heated at 1300 C.

The remaining celsian and hexacelsian powder was used for the design of experiments shown in Table 7. The results of the design of experiments are shown in Figure 26.

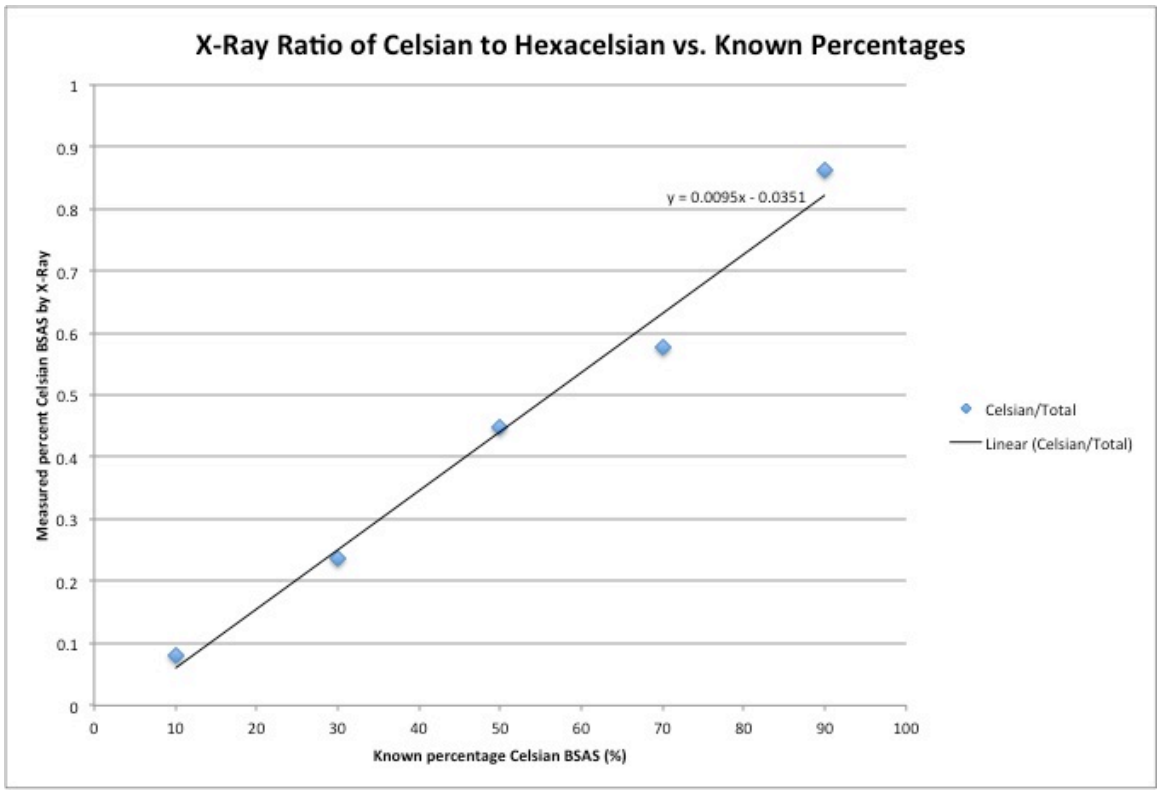

Figure 26. There is a linear relationship between the known and the measured percentages of celsian BSAS based on the heights of the peaks.

Since there is a linear and direct relationship between the ratio of the height of the (001) hexacelsian peak to the height of the (020) celsian peak with the known percentage, Equation 5 can be used to directly measure the percentage of celsian BSAS in the kinetic study.

$$\%\ Celsian\ BSAS = \frac{I_{(020)Celsian}}{I_{(020)Celsian} + I_{(001)Hexacelsian}}$$

$I_{(020)Celsian}$ is the intensity of the peak at 13.593° [25], and $I_{(001)Hexacelsian}$ is the intensity of the peak at 11.447° [26]. Figure 27 shows the increase of the percent of celsian BSAS over time for each temperature.

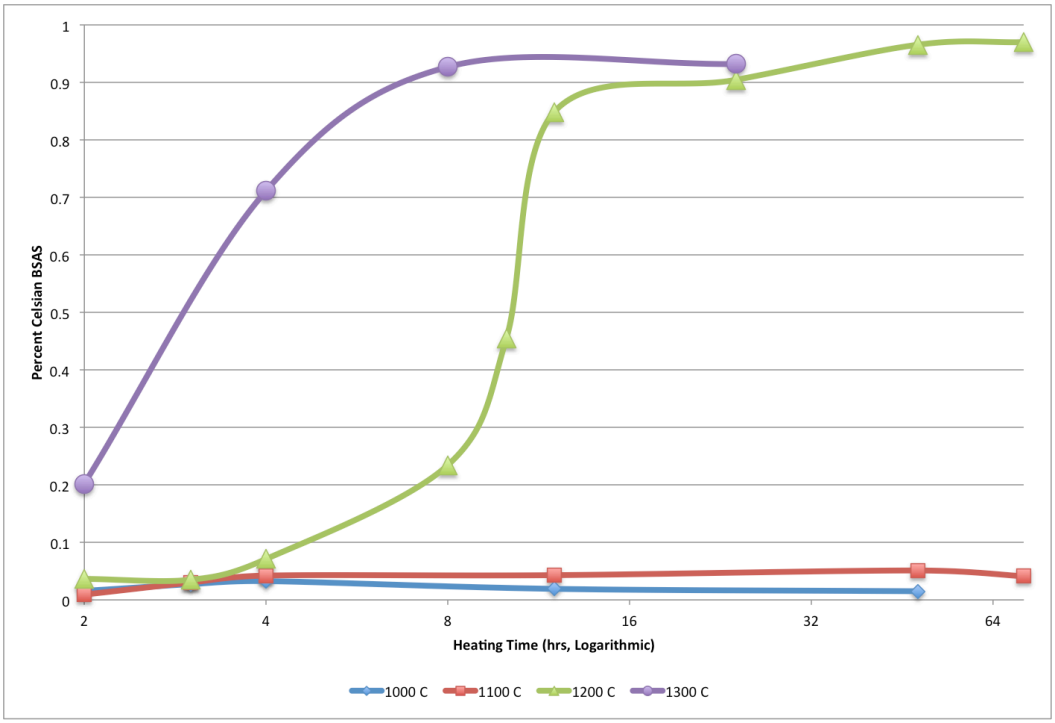

Figure 27. Time-percentage profile of celsian BSAS for each heat-treatment temperature.

3.5 Plasma Spraying of BSAS

The phases of the plasma-sprayed samples were analyzed using x-ray diffraction. The x-ray spectra revealed that all experiments resulted in an amorphous coating. The celsian powder that was sprayed at 37.5 SLM argon, 6.0 SLM hydrogen, and 550 amperes showed some signs of unmelted celsian BSAS.

The spray distance plays an important role in the deposition of the coating. All coatings sprayed at 70 and 100 mm showed a lot of cracks on the surface. These cracks are probably the

result of a higher velocity and larger impact energy, causing an increased deposition stress. The increased deposition stress was enough to fracture the coating. The two coatings sprayed at 170 mm showed no surface cracking.

Sample 3 (37.5/6.0/550, SD=170 mm, 6 passes) was heat-treated for 48 hours at 1200 °C., with a ramp rate of 4°C/minute to prevent thermal shock that would cause delamination. X-ray diffraction showed that the phase of the coating was hexacelsian, which contradicts the kinetic study in section 3.4. The x-ray spectra for Sample 3 are shown in Figure 28.

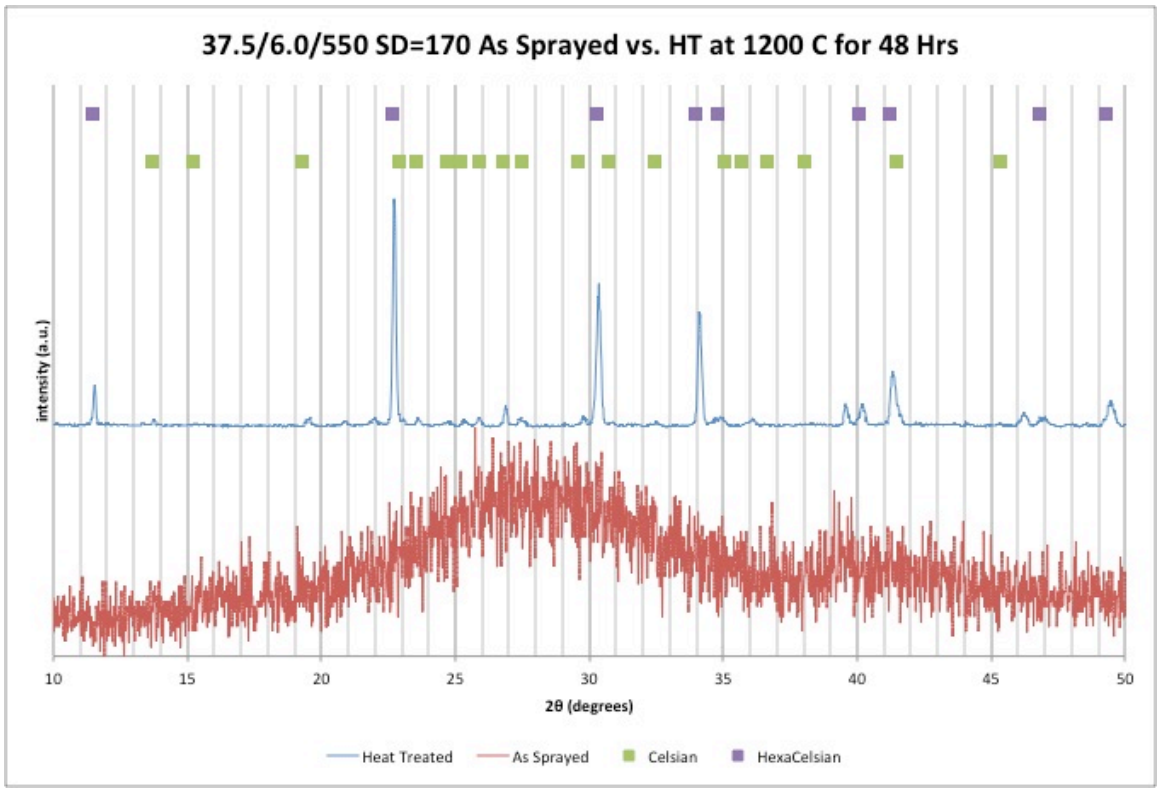

Figure 28. X-ray spectra of sample 3, both as-sprayed and heat-treated at 1200 C for 48 hours.

Further heat treatment experiments were done on Samples 6 and 9 (37.5/6.0/650, SD = 100, 5 passes, Hexacelsian and Celsian, respectively). Both were heat treated for 9999 minutes (166.7

hours) to see if it was possible to attain a fully celsian coating. Figures 29 and 30 show the x-ray spectra of the heat-treated Sample 6 and Sample 9, respectively.

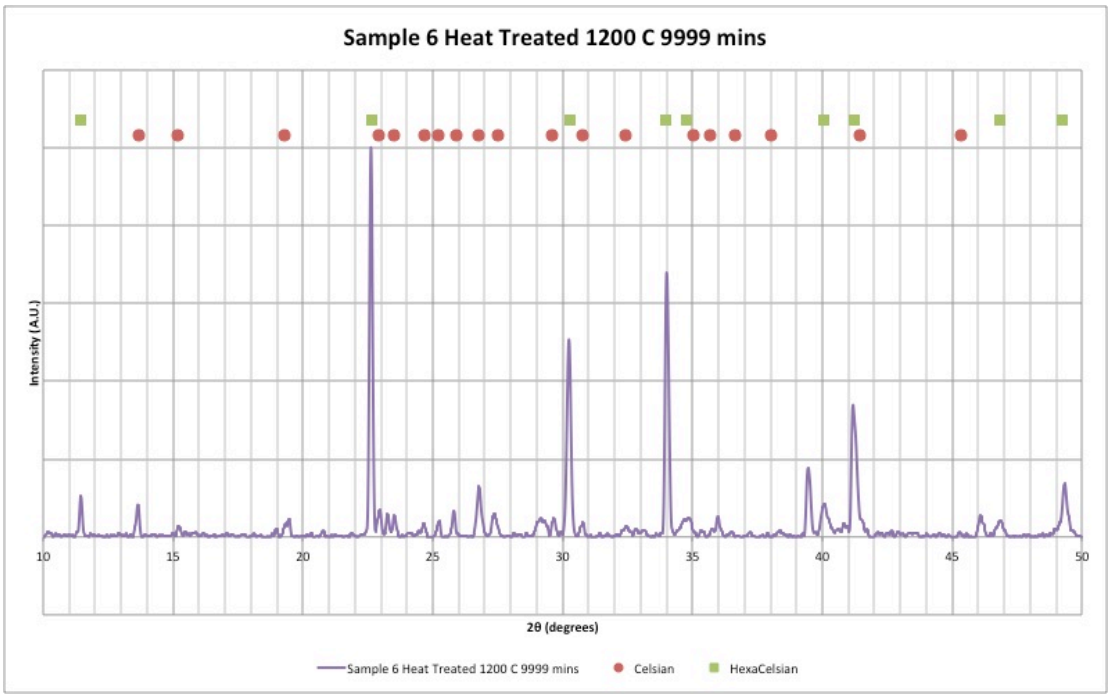

Figure 29. X-ray spectra of plasma sprayed hexacelsian BSAS heat-treated at 1200 C for 9999 mins.

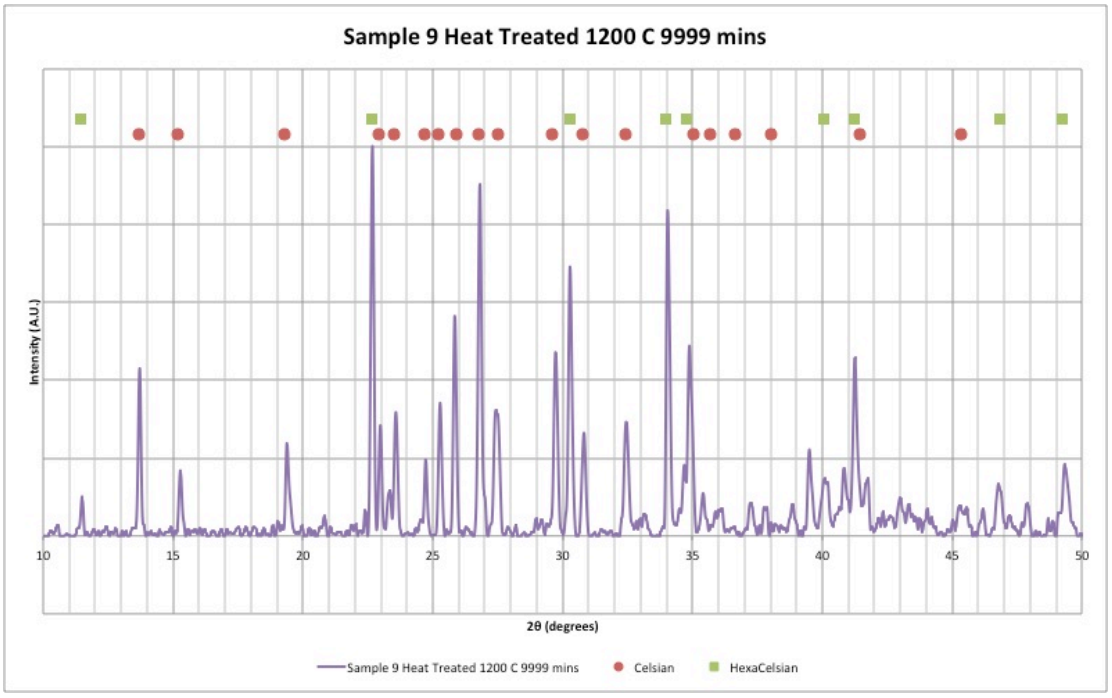

Figure 30. X-ray spectra of plasma sprayed celsian BSAS heat-treated at 1200 C for 9999 mins.

Despite heat-treating the coating for the maximum allowed time by the furnace, it was still not possible to achieve a fully celsian coating. However, it seems that the plasma sprayed celsian powder yielded a larger percentage of celsian BSAS in the coating than the plasma sprayed hexacelsian coating. This may be due to the celsian powder not fully melting during plasma spraying, despite a highly amorphous structure, and the remaining celsian crystals acted as a nucleation agent for the celsian phase transformation.

The images shown in Figure 31 (a, b) show the microstructures of the coatings sprayed from a distance of 170 mm, samples 1 and the heat-treated sample 3, respectively. Because the coating was sprayed from such a long distance, the particles may have solidified before they deposited onto the substrate. Because the particles are unmelted, they do not flatten like a molten particle does, and the resulting coating has high porosity. Figure 32 shows a sample sprayed from 100 mm. It was seen with the naked eye that there are lots of through-thickness cracks on the coating.

However, because this coating is much more dense than the ones form samples 1 and 3, it may be a better EBC.

a) 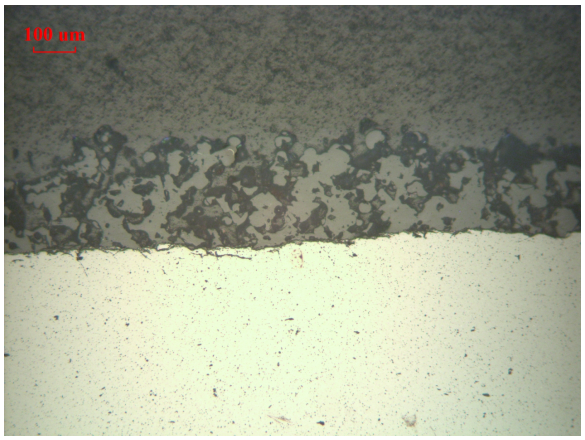

b) 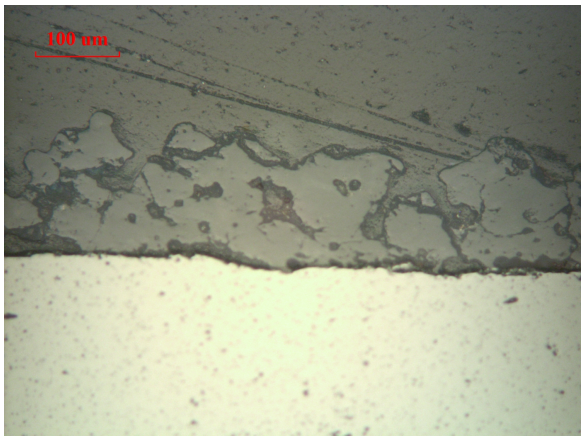

Figure 31. a) is the as-sprayed coating from 170 mm at 100X magnification. b) is the heat-treated coating at 200X.

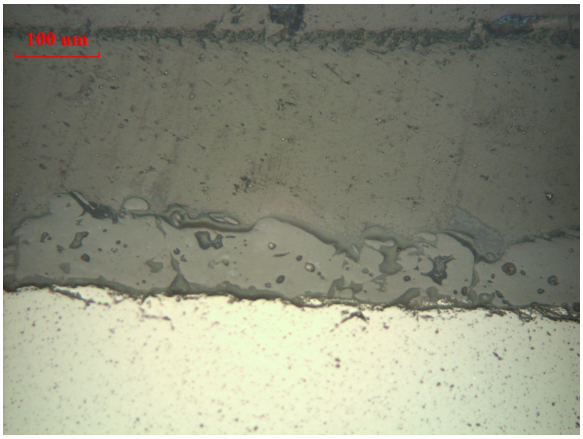

Figure 32. Sample 7 (section 2.7). The coating is much more dense than when sprayed at 170 mm. (200X)

4 Future Work

4.1 Sol-Gel Synthesis

Due to the lack of reactant materials for the sol-gel process, further experimentation may be required. Because the sintered mixture of yttria-monosilicate has a much higher CTE than its theoretical counterpart, sol-gel synthesized yttria-monosilicate will lead to a more stable coating due to its increased homogeneity.

Sol-gel synthesized yttria-disilicate has not yet been achieved, but a linear design of experiments to determine the percent of both yttria-monosilicate and yttria-disilicate with respect to the amount of yttrium nitrate or TEOS will help to determine how much of each reactant is required to obtain both pure yttria-monosilicate and disilicate.

4.2 Kinetics of BSAS

Due to the limit of the temperature of the tube furnace provided, only 4 experiments were performed on a temperature above 1200 °C. It is necessary to perform more heat-treatments at different temperatures ranging from 1200 °C to 1400 °C.

More heat-treatments also need to be done for the transition ranges between hexacelsian and celsian BSAS a. With the results of these experiments, a the kinetics of the transformation can be found based on the Avrami equation [10]:

$$\ln(-\ln(1-x)) = \ln k + n \ln t$$

Mixing known percentages of pure hexacelsian and celsian BSAS, and obtaining the x-ray spectra of these percentages through extrapolation, would provide a framework to find the percentage of heat-treated BSAS during the transition. The percentage of celsian BSAS, x, would be a function of the Avrami parameters *k* and *n,* and the heat-treatment time *t* [10]. Figure 33 shows the kinetic study of BSAS done by Harder, *et al.*, [10]. The Avrami parameters are found based on the vertical axis intercept for *k*, and the slope of the curve for *n*.

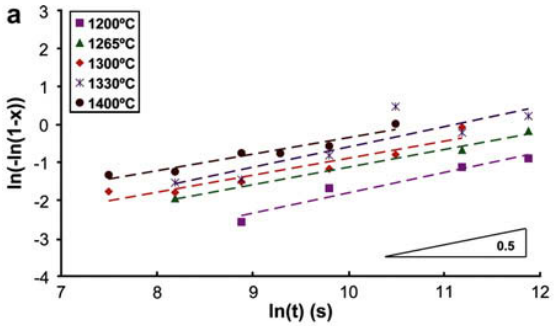

Figure 33. Kinetic study of BSAS as performed by Harder, *et al.* [10]

4.3 Plasma Spraying of BSAS

The x-ray spectra of all the plasma-spray experiments show that all plasma sprayed BSAS results in an amorphous coating, and x-ray diffractometry after heat-treatment reveals that the transformation kinetic of the coating may be slower than the transformation kinetic of the raw material, which contradicts what Harder, *et al*., suggests [10]. This needs to be inspected further by more plasma spraying and heat-treatment experiments, and the effect of the plasma spray and heat-treatment parameters on the microstructure and the phase of the BSAS coatings.

Another possibility of obtaining celsian BSAS by plasma spraying by using the plasma flame to heat-treat the coating after the spraying is completed. Another option is spraying it on to a sample inside a furnace at a high temperature. Like this, the sample does not need to undergo additional residual stress after cooling, and the phase transformation of BSAS from amorphous to celsian can occur *in-situ*.

5 Conclusion

Yttria-silicate mixtures and BSAS have the material properties necessary to make a good EBC. However, thermally spraying these materials require the correct processing outside of plasma spraying.

Yttria-silicate has low oxygen permeability and a CTE that matches the substrate silicon carbide. However, yttria-monosilicate does not bond well to SiC because the actual CTE is much higher than its theoretical CTE. This is also an issue with duplex coatings, where the CTE difference between yttria-monosilicate and yttria-disilicate can cause propagation of the through thickness crack when undergoing thermal cycling.

Sol-gel offers a promising solution to this problem. Yttria-monosilicate prepared by sol-gel has a better homogeneity than sintered yttria and silica. However, controlling the ratio of yttria to silica is very difficult as external variables can easily influence it.

BSAS is an alternative material for an EBC on SiC. However, the amorphous and hexacelsian phases of BSAS have a high CTE. Kinetic studies have shown that a lot of heat applied over a long period of time can change the BSAS to the celsian phase, which has a CTE that matches SiC.

The plasma spraying of BSAS yields an amorphous coating. The kinetics of a BSAS coating is slower than a BSAS powder, making it more challenging to obtain a celsian BSAS coating.

References

[1] A. Bennett, "Requirements for engineering ceramics in gas turbine engines," *Materials Science and Technology,* vol. 2, pp. 895-899, 1986.

[2] B. J. Harder, J. D. Almer, C. M. Weyant, K. N. Lee, and K. T. Faber, "Residual Stress Analysis of Multilayer Environmental Barrier Coatings," *Journal of the American Ceramic Society,* vol. 92, pp. 452-459, 2009.

[3] E. J. Opila and R. E. H. Jr., "Paralinear Oxidation of CVD SiC in Water Vapor," *Journal of the American Ceramic Society,* vol. 89, pp. 197-205, 1997.

[4] K. N. Lee, D. S. Fox, and N. P. Bansal, "Rare earth silicate environmental barrier coatings for SiC/SiC composite and Si3N4 ceramics," *Elsevier,* vol. 25, pp. 1705-1715, 2005.

[5] K. N. Lee, R. A. Miller, and N. S. Jacobson, "New Generation of Plasma-Sprayed Mullite Coatings on Silicon Carbide," *Journal of the American Ceramic Society,* vol. 78, pp. 705-710, 1995.

[6] W. J. Lackey, D. P. Stinton, G. A. Cerny, A. C. Schaffhauser, and L. L. Fehrenbacher, "Ceramic coatings for advanced heat engines - A review and projection," *Advanced Ceramic Materials,* vol. 2, pp. 23-34, 1987.

[7] Z. Sun, M. Li, and Y. Zhou, "Thermal properties of single-phase Y2SiO5," *Journal of the European Ceramic Society,* vol. 29, pp. 551-557, 2009.

[8] M. Aparicio and A. Duran, "Yttrium Silicate Coatings for Oxidation Proteciton of Carbon-Silicon Carbide Composites," *Journal of the American Ceramic Society,* vol. 83, pp. 1351-1355, 2000.

[9] E. M. Levin, C. R. Robbins, and H. F. McMurdie, *Phase Diagrams for Ceramists 1969 Supplement*. Columbus, Ohio: The American Ceramic Society, 1969.

[10] B. J. Harder and K. T. Faber, "Transformation kinetics in plasma-sprayed barium and strontium-doped aluminosilicate," *Scripta Materialia,* vol. 62, pp. 282-285, 2009.

[11] K. N. Lee, D. S. Fox, J. I. Eldridge, D. Zhu, R. C. Robinson, N. P. Bansal, and R. A. Miller, "Upper Temperature Limit of Environmental Barrier Coatings Based on Mullite and BSAS," *Journal of the American Ceramic Society,* vol. 86, pp. 1299-1306, 2004.

[12] C. M. Weyant, "Tantalum Oxide-Based Plasma-Sprayed Environmental Barrier Coatings," Doctor of Philosophy, Materials Science and Engineering, Northwestern University, Evanston, Illinois, 2004.

[13] S. Bose, *High Temperature Coatings*. Oxford, UK: Butterworth-Heinemann, 2007.

[14] J. R. Davis, *Handbook of Thermal Spray Technology*. Materials Park, OH: ASM International, 2005.

[15] (2007). *Plasma Spraying*. Available: http://www.fst.nl/en/page00043.asp

[16] J. Koutsky, "High velocity oxy-fuel spraying," *Materials Processing Technology,* vol. 157-158, pp. 557-560, 2004.

[17] (2007). *High Velocity Oxy Fuel (HVOF)*. Available: http://www.fst.nl/en/page00042.asp

[18] S. Deshpande, A. Kulkarni, S. Sampath, and H. Herman, "Application of image analysis for characterization of porosity in thermal spray coatings and correlation with small angle neutron scattering," *Surface & Coating Technologies,* vol. 187, pp. 6-16, 2004.

[19] J. D. Wright and N. A. J. M. Sommerdijk, *Sol-Gel Materials Chemistry and Applications*. Boca Raton, FL: CRC Press, 2001.

[20] M. Diaz, I. Garcia-Cano, S. Mello-Castanho, J. S. Moya, and M. A. Rodriguez, "Synthesis of nanocrystalline yttrium disilicate powder by a sol-gel method," *Journal of non-crystalline solids,* vol. 289, pp. 151-154, 2001.
[21] J. S. Moya, M. Diaz, C. J. Serna, and S. Mello-Castanho, "Formation of Nanocrystalline Yttrium Disilicate Powder by an Oxalate Gel Method," *Jorunal of the European Ceramic Society,* vol. 18, pp. 1381-1384, 1998.
[22] D. K. Mauritz. Sol-Gel Chemistry.
[23] "Y2Si05," 41-0004, Ed., ed: JCPDS-International Centre for Diffraction Data, 2000.
[24] (2011). *Yttrium Oxide (Y2O3)*. Available: http://www.goodfellow.com/E/Yttrium-Oxide.html
[25] "Ba0.75Sr0.25Al2Si208," 38-1451, Ed., ed: JCPDS-International Centre for Diffraction Data, 2000.
[26] "Ba0.9Sr0.1Al2Si208," 26-0182, Ed., ed: JCPDS-International Centre for Diffraction Data, 2000.